Observation of Nanoscale Cooling Effects by Substrates and the Surrounding Media for Single Gold Nanoparticles under CW-Laser Illumination

Kenji Setoura, Yudai Okada, Daniel Werner, and Shuichi Hashimoto*

Department of Optical Science and Technology, The University of Tokushima, Tokushima 770-8506, Japan

ABSTRACT Understanding the nanoscale heating-induced local thermal response is important but hampered by lack of information on temperatures at such small scales. This paper reports laser-induced heating and thermal equilibration of metal nanoparticles supported on different substrates and immersed in several media. We use single-particle spectroscopy to monitor nanoparticle temperature rises due to laser excitation. Because of changes in the refractive index of the surrounding medium, the scattering spectrum of the gold nanoparticles undergoes a shift that is related to the temperature of the system. We find that the temperature increase depends on both the surrounding medium and the supporting substrate. We furthermore model the nanoparticle temperature using a simplified 1-D heat conduction model with an effective thermal conductivity that takes both substrate and environment into account. The results from this model are also compared to a more detailed 2-D heat transfer analysis. The results presented here are quite new and important to many plasmonic nanoparticle applications where the strong absorption cross section of the nanoparticles leads to a significant temperature rise. In particular, the current work introduces an analysis that can be easily implemented to model the temperature of a nanoparticle supported on a substrate, as is the case in many single-particle measurements.

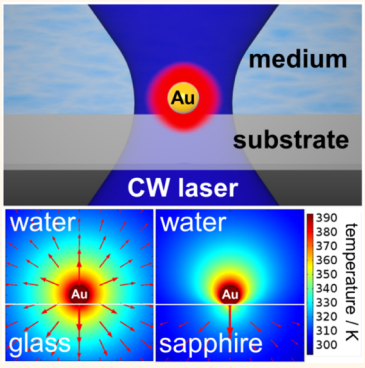

KEYWORDS: single gold nanoparticle · continuous wave laser heating · temperature measurement · effective thermal conductivity · substrate · medium

Plasmonic nanoparticles (NPs) have emerged as nanoscale heat sources, the heating power of which can be controlled remotely through optical excitation.[1−3] Simultaneously, heat transfer from the NPs enables the surrounding medium to be heated. Within the limited time scales imposed by irradiation periods, medium heating is confined to a nanospace accompanied by a temperature gradient. This unique attribute of plasmonic heating-related energy deposition has potential applications to photothermal cancer therapy and nanofabrication.[4−7]

To gain deeper insight into the photothermal response of plasmonic NPs, a single-particle approach is preferred. Single-particle spectroscopy has a big advantage in tracking the properties and reactions of individual NPs, including the effects of the ambient environment, by monitoring continuous spectral peak shifts and their changes in shape. Such observations are not possible with ensemble measurements that are subject to distributions in particle size and shape as well as inhomogeneous spectral broadening.[8] The single-particle approach has another advantage from tracking and manipulating single NPs with high temporal and spatial resolutions. Single-particle studies using plasmonic heating by continuous wave (CW)-laser illumination have been reported. For instance, bubble-induced damaging of polyelectrolyte films that mimic cell membranes or biological tissues has been demonstrated.[9] Thermal imaging of nanostructures has also been conducted using quantitative optical phase analysis.[10] Moreover, nanochannel milling in polyvinyl alcohol films driven by a

* Address correspondence to hashichem@tokushima-u.ac.jp.

Received for review June 6, 2013 and accepted August 25, 2013.

Published online August 26, 2013
10.1021/nn402863s

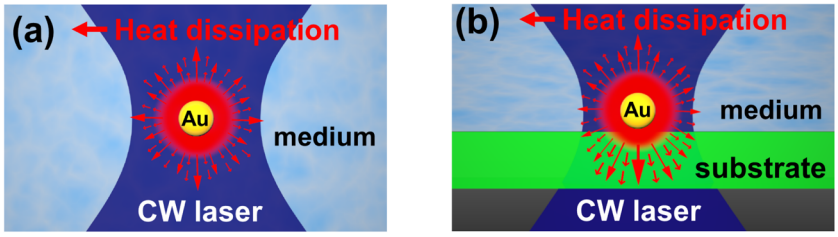

Scheme 1. Schematic illustrations of heat dissipation for a Au NP under steady-state laser illumination, in a homogeneous medium (a) and supported on a substrate and immersed in a medium (b).

laser-manipulated Au NP, as well as laser embedding of a Au NP in polymeric films, has been developed.[11,12] However, *in situ* measurements of temperature of these Au NPs are limited to only a few cases.[13−15]

We have recently devised a method to measure the temperature of a single Au NP under CW-laser illumination.[16] Based on spectral calculations applying Mie theory, experimental scattering peak shifts of localized surface plasmon resonance (LSPR) bands were exploited to estimate particle temperatures in the range 300−600 K with an accuracy of ±20 K. The method has the advantage of acquiring particle temperatures without using a calibration coefficient such as a temperature transfer coefficient or relying on thermophysical calculations that contain unknown parameters.[13] The particle temperatures were determined in a way that is not affected by the spatial resolution of the optical setup. We also observed that the surrounding media such as water and glycerol affect the spectral shifts through heating-induced refractive index changes. This result prompted us to investigate medium and substrate effects on particle temperature. Essentially, both the surrounding medium and substrate act as a heat sink, the capability of which is determined by their thermal conductivities.

To estimate the temperature of plasmonic nanostructures under steady-state heating, the most convenient way is to apply the one-dimensional (1-D) heat conduction equation.[17] The equation can be applied to a spherical NP immersed in a homogeneous medium (Scheme 1a). However, unless particles are suspended by a laser-trapping technique, NPs are usually supported on a substrate. Heat transfer for this system is complicated because of the presence of the substrate (Scheme 1b). In applying the 1-D heat conduction equation to such a complex system, the averaged thermal conductivity of medium and substrate is used as the thermal conductivity of the medium.[9,13] This averaging is acceptable only when a small thermal conductivity disparity exists, as for the water/glass system. However, there have been no studies demonstrating the accuracy when using averaged thermal conductivities. In particular, it is not clear whether the concept of averaged thermal conductivity is applicable to cases in which a greater thermal conductivity disparity between medium and substrate is expected.

In this paper, we show, for a single Au NP, observation of a substrate-medium-dependent temperature increase that is proportional to the intensity of the illuminating laser. Substrate and medium were found to contribute significantly to particle cooling that governs the efficiency of laser heating. As a result, we made a reasonable estimation of the effective thermal conductivities k_{eff} for several medium−substrate systems by applying the 1-D heat transfer model. This is only possible for a method that can properly estimate the temperature of a particle under laser illumination. Herein, we evaluated the adequacy of the experimental k_{eff} based upon the numerical calculations of particle temperatures.

RESULTS AND DISCUSSION

Temperature Estimation of a Single Au NP under CW-Laser Illumination. Laser illumination enables Au NPs to undergo temperature increases, reaching a steady-state temperature resulting from plasmonic heating followed by heat dissipation to the surrounding medium. This causes LSPR spectral damping.[18,19] This damping is accompanied by spectral peak shifts from which temperature information was previously extracted.[16] For Au NPs on a substrate immersed in a medium, heat transfer is a complicated process because of the presence of three interfaces: the NP−medium, the NP−substrate, and the medium−substrate. Thus, to track heat transfer processes in such a system, temperature information for the particle is crucial. The advantage of the scattering spectral method over the fluorescence sensor approach is that it is possible to access particle temperature directly without being obscured by the diffraction-limited volume of the focal spot.[16] Here, we describe our attempt to observe substrate-dependent particle temperatures for substrates with different thermal conductivities.

Figure 1 shows the scattering spectra from a single 100-nm-diameter Au NP (see Supporting Information, Figure S1 for TEM images) supported on three substrates, glass, CaF_2, and sapphire, that were immersed in water (for thermophysical and optical properties of substrates and media, see Supporting Information, Table S1 and Figure S2); the spectra were obtained under 488 nm CW-laser illumination. Upon excitation, substrate-dependent peak shifts were clearly observed.

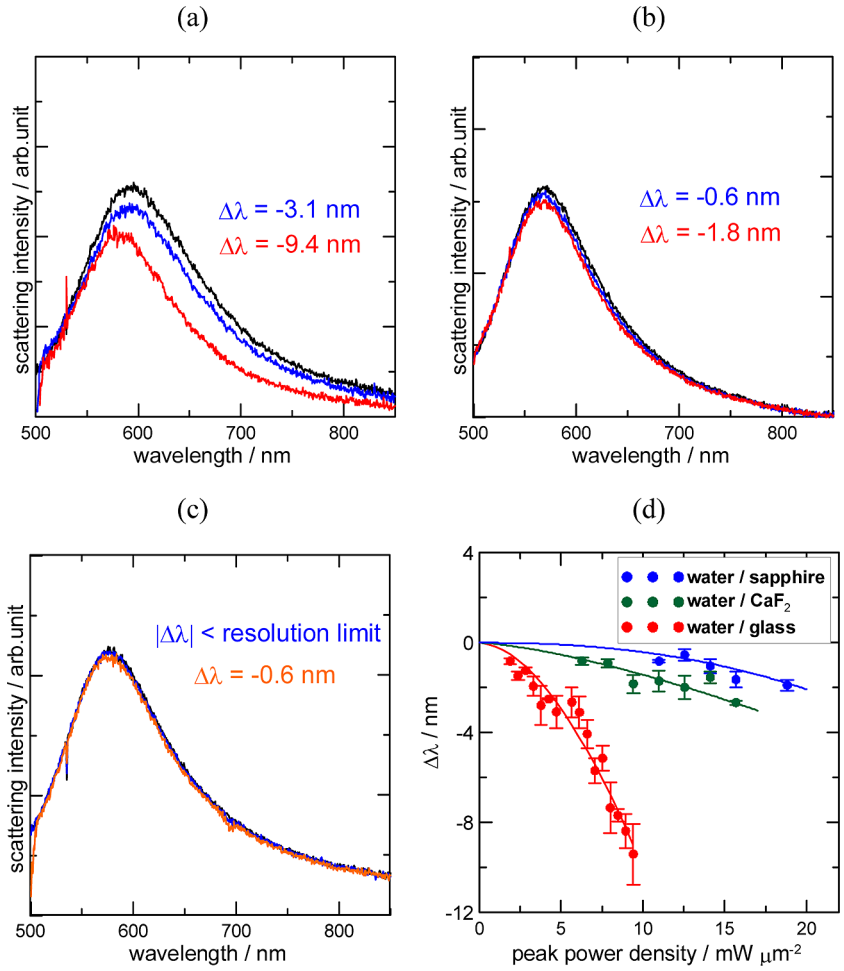

Figure 1. Experimental scattering spectral changes of a single 100-nm-diameter Au NP supported on glass, CaF_2, and sapphire in water: (a) water/glass, (b) water/CaF_2, and (c) water/sapphire. Black curves indicate spectra without CW-laser illumination; blue, red, and orange curves indicate spectra from excitation at 4.7, 9.4, and 11.0 mW μm^{-2}. Particles with similar diameters were selected for the spectral measurements (scattering peaks at 583 $\pm$ 3 nm (water/glass), 571 $\pm$ 1 nm (water/CaF_2), 578 $\pm$ 1 nm (water/sapphire)); (d) curves of the peak shift $\Delta\lambda$ as a function of laser peak power density for the above three systems. Three 490 nm cutoff long-pass sharp edge filters were used in the measurements. Note that 1.0 mW $\mu m^{-2} = 10^5$ W $cm^{-2} = 10^9$ W m^{-2}.

For instance, at the excitation laser intensity of 4.7 mW μm^{-2}, besides the distinctive damping, an appreciable blue shift (Figure 1a) was observed in water/glass. In contrast, the spectral changes at the same excitation intensity in water/CaF_2 and water/sapphire were not as remarkable (see Figure 1b and c). The origin of the blue shift is ascribed to temperature-dependent variation in refractive index of the surrounding water (Supporting Information, Figure S2a). The various substrate-dependent shifts originate from the variation in thermal conductivities of the substrates. As a result, the blue shifts in water/CaF_2 and water/sapphire were noticeably suppressed because these substrates have thermal conductivities much higher than glass, and the temperature increase of a supported Au NP is lower than in the water/glass system. The peak shifts and $\Delta\lambda$ *vs* laser peak power density curves in the above three systems are summarized in Figure 1d; parabolic curves are drawn because the temperature dependence of the refractive index for water is parabolic (Supporting Information, Figure S2a). Fitting functions for the parabolic curves are given in the Supporting Information, S3.

When the substrates were immersed in glycerol instead of water, we again observed blue shifts, the magnitude of which increased with increasing laser intensity (Figure 2). Note here that the curves are linear because of the linearity of the refractive index with temperature (Supporting Information, Figure S2a). Larger $\Delta\lambda$ values were observed in glycerol, a reflection of its lower thermal conductivity and d*n*/d*T* values than water. Contrastingly, smaller red shifts of the scattering spectra were observed in air as peak power density increased (Figure 3). The observed red shifts are ascribed to an intrinsic property of Au NP that arises because of changes in the conduction electron scattering frequency caused by temperature increases.[18,19] Note that the temperature coefficient of the refractive index of air is negligibly small. A possible cause for the scattering spectral shifts is that an adsorbed water layer with a thickness of a few nanometers forms on

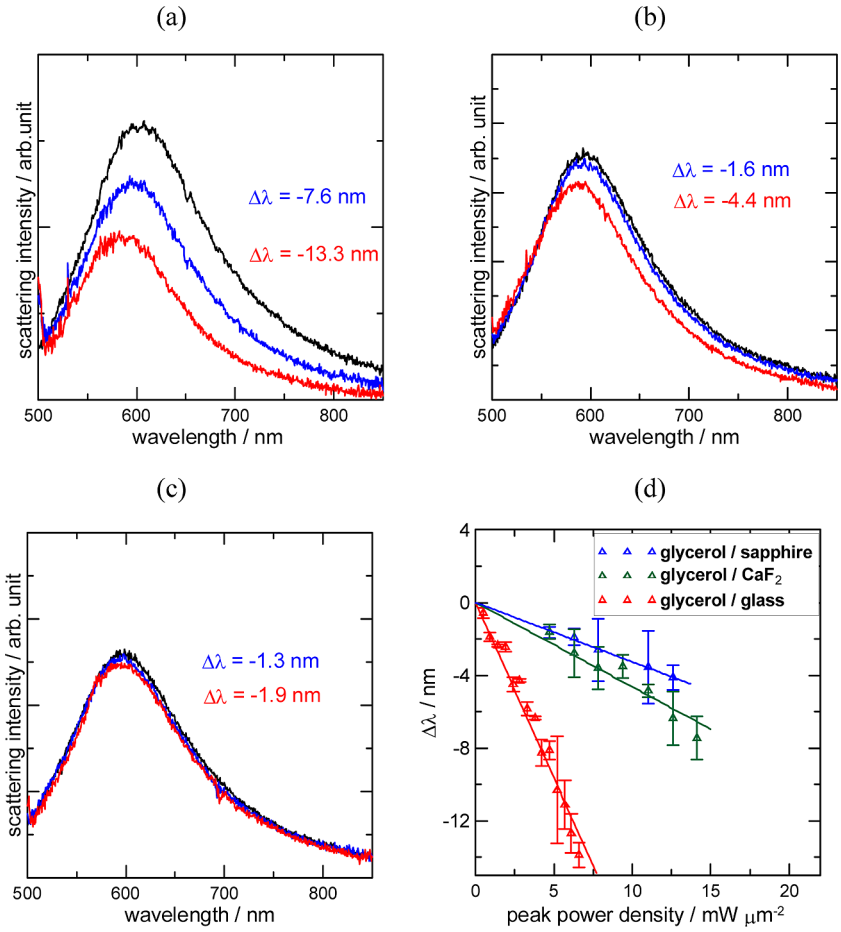

Figure 2. Experimental scattering spectral changes on laser illumination of a single 100 nm diameter Au NP supported on glass, CaF_2, and sapphire substrates submerged in glycerol: (a) glycerol/glass, (b) glycerol/CaF_2, and (c) glycerol/sapphire. Blue shifts were observed. Black lines show the spectra without laser illumination. Blue and red lines show the spectra on excitation with intensities of 4.7 and 6.6 mW μm^{-2}. Au particles with original scattering peaks of 605 $\pm$ 1.0, 592 $\pm$ 2.4, and 598 $\pm$ 1.0 nm were selected in glycerol/glass, glycerol/CaF_2, and glycerol/sapphire. (d) Peak shifts, $\Delta\lambda$, as a function of laser peak power density for the three systems mentioned above.

the substrate surface in an ambient atmosphere.[20,21] Supposing that the substrate heating causes the vaporization of adsorbed water, blue shifts can result if the refractive index around a Au NP is decreased. However, this was not observed in air; thus, the effect of coadsorbed water on the substrates is negligibly small. Among the three substrates, sapphire exhibits the strongest cooling effect, followed by CaF_2 and then glass. In short, the results showed clearly the quantitative difference in the cooling effects of the substrate and medium during plasmonic heating of a Au NP in terms of the scattering spectral peak shifts, $\Delta\lambda$.

Estimation of Effective Thermal Conductivities for Various Medium/Substrate Pairs. The scattering spectral peak shifts, $\Delta\lambda$, were measured at various excitation laser intensities (peak power densities) for the three selected substrates in air, water, and glycerol, thus enabling estimates of particle temperatures, T_p. Previously, a method was devised for estimating the temperature of a Au NP under CW-laser illumination.[16] The particle temperatures were determined by comparing the peak positions of experimental scattering spectra with those of the temperature-dependent scattering spectra. The temperature-dependent LSPR scattering spectra of a Au NP were obtained using Mie theory.[22,23] In the Mie calculation, the temperature-dependent dielectric functions were obtained by fitting to Otter's experimental values for the range 450−700 nm at four temperatures: 283, 583, 843, and 1193 K.[24] In addition, the refractive index gradients of the media, water, and glycerol were taken into consideration in T_p calculations. The temperature coefficients for the refractive indices of substrates are an order of magnitude smaller than those of water and glycerol. Therefore, we considered that the temperature-induced refractive index changes of substrates contribute negligibly to the scattering spectral shifts (Supporting Information, Figure S4). The method gives a direct measure of the temperature increase caused by laser heating, irrespective of the spatial resolution of the optical setup. The particle temperatures thus obtained can be used to identify cooling effects as differences in T_p when various substrates and media are used.

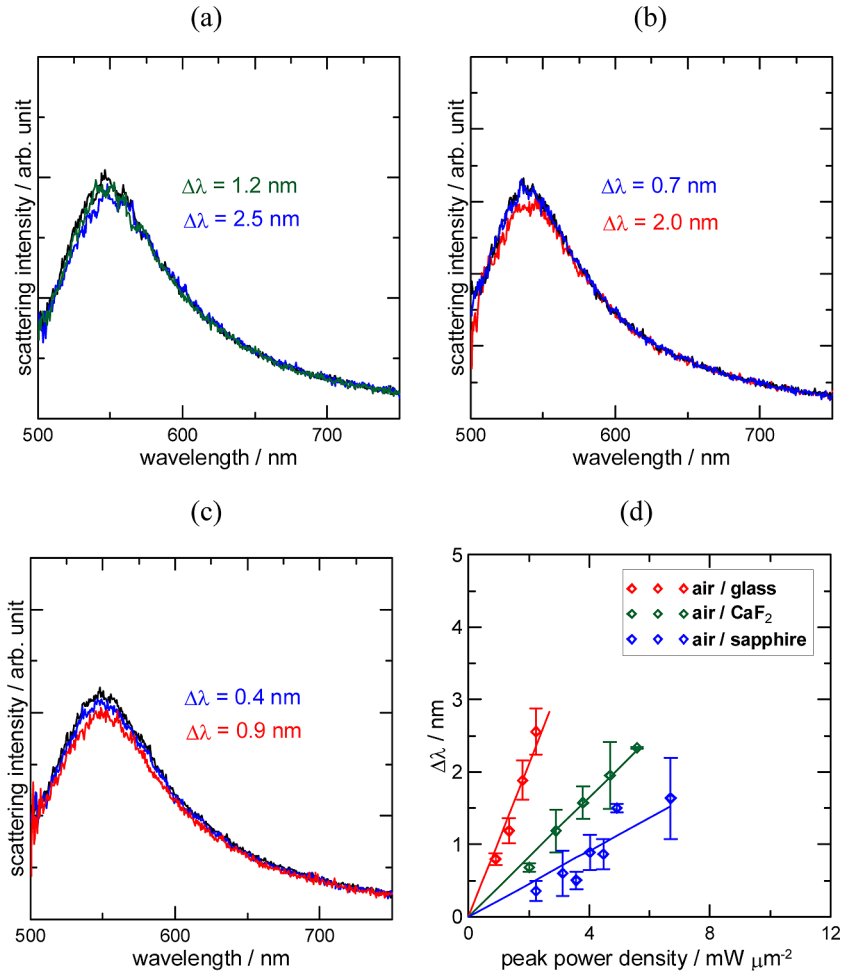

Figure 3. Experimental scattering spectral changes on laser illumination of a single 100-nm-diameter Au NP supported on glass, CaF_2, and sapphire substrates in air: (a) air/glass, (b) air/CaF_2, and (c) air/sapphire. Here, red shifts were observed. Black lines show the spectra without laser illumination. Green, blue, and red solid lines show the spectra on excitation at the laser powers of 1.3, 2.2, and 4.5 mW μm^{-2}. Particles with original scattering peaks of 549 $\pm$ 1.0, 540 $\pm$ 1.0, and 541 $\pm$ 1.0 nm were selected in air/glass, air/CaF_2, and air/sapphire. (d) Peak shifts, $\Delta\lambda$, as a function of laser peak power density in the above three systems.

An analytical formula for a simple 1-D heat conduction equation has been established to estimate the local heating by a NP in a homogeneous medium (Scheme 1a). The temperature profile, $T(r)$[K], is given by[1−3,13,15,17,25]

$$T(r) = T(\infty) + \frac{C_{abs} I}{4\pi k r} \quad (r \geq a: \text{ particle radius}) \qquad (1)$$

where r [m] is the radial coordinate, $T(\infty)$ [K] ambient temperature, C_{abs} [m^2] absorption cross section of Au NP at the excitation wavelength, and I [W m^{-2}] peak power density of the excitation laser. To apply the 1-D heat conduction equation to a complex system consisting of NP, medium, and substrate, the thermal conductivity of the surroundings (medium and substrate) was represented by an effective (averaged) thermal conductivity $\bar{k}$ [W m^{-1} K^{-1}],[9,13]

$$\bar{k} = \frac{k_{med} + k_{sub}}{2} \qquad (2)$$

with k_{med} and k_{sub} denoting the thermal conductivities of the medium and substrate, respectively. In addition, a finite interface resistivity is defined that enables a finite temperature discontinuity to occur at the interface between the NP surface and the surrounding medium. This parameter plays a main role in describing the observed temperature drop at this interface during femtosecond/nanosecond pulsed-laser excitation.[26−30] This parameter, however, can be negligible in steady-state heating of Au NPs, as temperature drops are slight at the NP/medium interface (see Supporting Information, Figure S5, temperature profile, $T(r)$, with/without finite interface resistivity). In the derivation of eq 1, the particle temperature was assumed constant because of the sufficiently high thermal conductivity of gold (314 W m^{-1} K^{-1}). Thus, for particle radius a, $T(a) = T(r < a) = T_p$ is implicitly assumed.

Here, we look at our experimental T_p and its dependency on the substrates and their intrinsic thermal conductivities. Figure 4 shows the peak power density *vs* T_p, for three substrates in water, estimated from the experimental laser power-dependent $\Delta\lambda$ (a), compared with the same relationship using a calculation

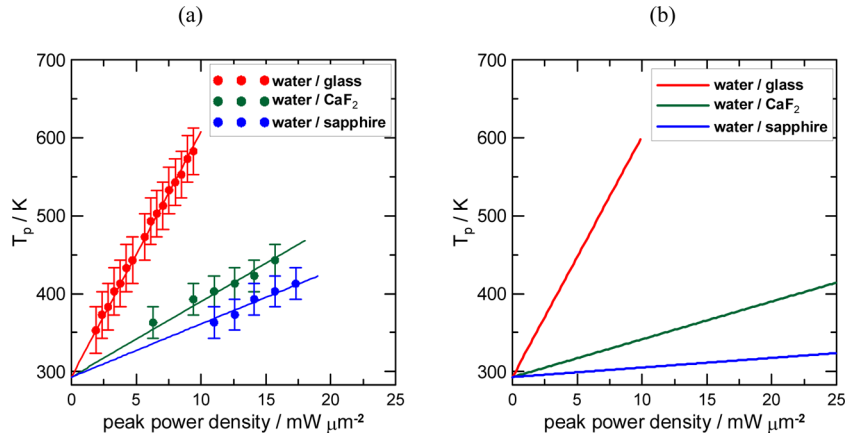

Figure 4. Laser peak power density *vs* T_p relationship estimated from experimental laser power-dependent $\Delta\lambda$ (a), in comparison with computational curves applying eq 1 with $\bar{k}$ instead of k (b) for a 100-nm-diameter Au NP supported on the three substrates in water. Errors in experimental temperature estimation: ±20 K. For the calculation using eq 1, the C_{abs} values given in Supporting Information, Table S4 and the $\bar{k}$ values listed in Table 1 were used.

applying eq 2 (b). The values of T_p are proportional to the laser intensities applied. Linear relationships between the experimental T_p and the laser intensity were observed also in other media, glycerol, and air (see Supporting Information, S6, for the three substrates in glycerol and air). The laser intensities were adjusted subject to $T_p < 600$ K to avoid softening or melting of the substrates (Supporting Information, Table S1).[16] Figure 4b was drawn by applying eq 1 using parameters described in the caption. Of these, C_{abs} values at 488 nm were obtained using Mie theory, for which effective medium refractive indices, ε_{eff}, were employed (Supporting Information, S7). The values obtained are similar to those obtained from the numerical calculation for a Au NP supported on three substrates (Supporting Information, S7). Both experimental and conventional T_p exhibit a linear relationship with laser intensity (Figure 4a and b). This suggests that the experimental T_p is adequately described by eq 1 and the experimental slope can be used to calculate k_{eff} for each medium/substrate pair. Thus, we determined k_{eff} values for various medium/substrate systems. The results are listed in Table 1. The experimental k_{eff} values in water/glass and glycerol/glass are in good agreement with conventional $\bar{k}$ values. In contrast, for other systems, a noticeable disagreement was observed. The difference between k_{eff} and $\bar{k}$ is large, especially for air as well as the sapphire substrate. The largest difference was observed for air/sapphire where $\bar{k}$ assumes 20 times the experimental k_{eff} value.

2-D Heat Conduction Analysis and Particle Temperature Calculation. The disagreement between k_{eff} and $\bar{k}$ might suggest a limitation in obtaining the effective medium thermal conductivity by averaging k_{sub} and k_{med} in the 1-D heat transfer analysis. This is because the heat transfer from the particles is spatially nonuniform. Therefore we applied 2-D heat conduction equations to visualize the heat transfer around a Au NP acting as a heat source while supported on a substrate and immersed in a medium. We considered a steady-state solution for a CW-laser heating to calculate the 2-D ($x-z$ plane) temperature distributions. The Poisson and Laplace forms of the heat conduction equations are

TABLE 1. Experimental k_{eff}, Conventional $\bar{k}$, and Computational k_{eff} by COMSOL (unit: W m^{-1} K^{-1})

medium/substrate	k_{eff} (exp *t*)	$\bar{k} = (k_{med}+k_{sub})/2$	k_{eff} (COMSOL)
air/glass	0.2 ± 0.1	0.51	0.23
air/CaF_2	0.6 ± 0.2	4.87	0.54
air/sapphire	1.1 ± 0.2	20.01	0.60
water/glass	0.8 ± 0.2	0.8	0.80
water/CaF_2	2.7 ± 0.5	5.16	3.25
water/sapphire	3.9 ± 1.0	20.3	5.43
glycerol/glass	0.6 ± 0.1	0.65	0.55
glycerol/CaF_2	2.5 ± 0.5	5.01	2.44
glycerol/sapphire	3.7 ± 1.4	20.15	3.85

$$k_{NP}\nabla^2 T(x,z) = Q(x,z) \quad (3)$$

$$k_{med}\nabla^2 T(x,z) = 0 \quad (4)$$

$$k_{sub}\nabla^2 T(x,z) = 0 \quad (5)$$

where k is the thermal conductivity, Q is the heat source, and the subscripts NP, med, and sub refer to the Au NP, the medium, and the substrate. The origin of the coordinates x (horizontal) and z (vertical) axes is set on the substrate surface, at the contact point of NP and the surface. Thus z^+ represents the medium side and z^- represents the substrate side. Equations 3–5 describe the heat conduction in the NP, the medium, and the substrate, respectively; the boundary condition at $(x^2 + (z - a)^2)^{1/2} = a$ (NP/medium interface) is

$$k_{NP}\partial_{x,z}T(a^+) = k_{med}\partial_{x,z}T(a^-), \quad T(a^+) = T(a^-) \quad (6)$$

where a^+ and a^- distinguish the inner and outer surfaces of the particle. The boundary condition at $z-0$(medium/substrate interface) is

$$k_{med}\partial_{x,z}T(z^+) = k_{sub}\partial_{x,z}T(z^-), \quad T(z^+) = T(z^-) \quad (7)$$

These parameters were basically the same as those used in analyzing the femtosecond laser excitation.[29]

Under steady-state heating, heat loss at each interface was assumed negligible because of a smaller contribution to the resistivity from the finite interface (Supporting Information, S5). For nanoscale laser heating of a substrate−single plasmonic nanostructure in a liquid medium, the free convective heat transfer has been demonstrated to be negligible.[31] In contrast, for micrometer-scale objects, convection should be taken into consideration. To solve numerically the 2-D temperature distribution of eqs 3−5, we employed COMSOL Multiphysics based on the finite element method (Supporting Information, S8). The temperature coefficient of the thermal conductivity of borosilicate glass substrate is negligible. However, the temperature coefficient is appreciable for CaF_2 and sapphire. Hence, we considered the temperature-dependent thermal conductivity of these substrates for the calculation (Supporting Information, Figure S2d and e).

We found that the results obtained by the numerical calculation depend on contact area, which in turn is a function of the separation between the particle and the substrate surfaces. The particles we employed in this study are regarded as spheres because of laser surface treatment (Supporting Information, S1, for TEM micrographs). Additionally, the substrates have an average surface roughness R_a of 0.1−0.2 nm, and a peak to valley roughness R_t of 1.0 nm, as determined by AFM measurements (Supporting Information, S9). The surface roughness of the substrates can be responsible for the particle−substrate separation. Because of difficulties in uniquely determining the separation experimentally, we calculated the heat conduction assuming three typical cases, as given pictorially in Scheme 2. Scheme 2a represents the point contact between the sphere and the smooth surface. Ideally, this model should give the best computational result. In Scheme 2b, a greater contact area than a point contact was assumed where a particle is trapped in a pocket on the substrate surface. In this case, we moved a Au NP sphere from the point contact position to the substrate side. Scheme 2c represents a model for separated particle−substrate, in a situation where a spherical Au NP sits on a spiky surface. In Scheme 2c, a lower thermal effect from the substrate can be predicted. The calculation with the separation model was made assuming the contact area has a thermal conductivity of the medium. The particle−substrate separation was set to 0.3 nm, which corresponds to a monolayer thickness of a solvent such as water to fill the space.[32] We used a separation smaller than 1 nm because Au

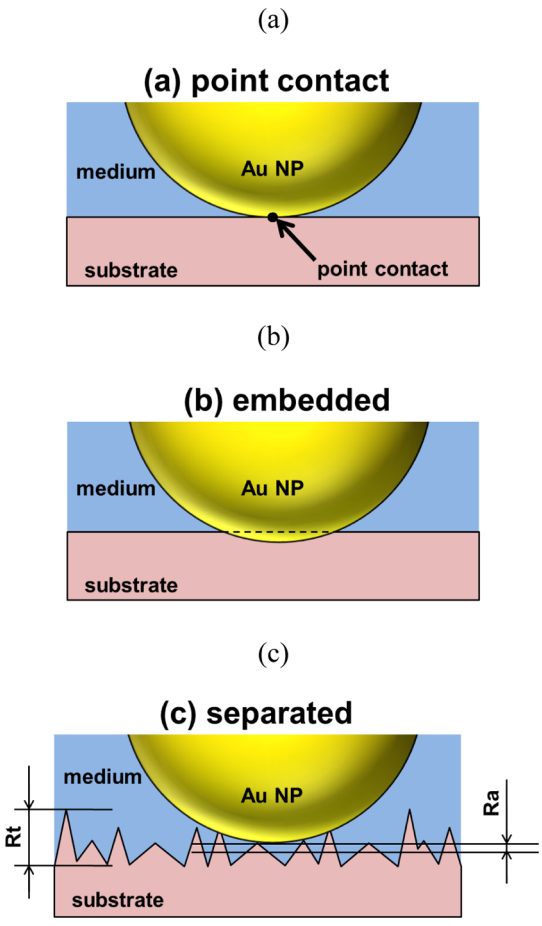

Scheme 2. Schematic illustrations for three types of particle surface−substrate surface separations: point contact, or 0 nm separation (a), partially embedded in the substrate (b), and separated (c). The Au NPs were assumed as a sphere based on the observation of TEM images. The surface roughness of the three substrates was determined by AFM measurements (Supporting Information, S9). The surface roughness of the substrates (the spiked surface filled with the medium) was assumed to be responsible for the origin of particle−substrate separations.

NPs tend to stay at stable positions on substrates with smaller roughness. We used the same value of 0.3 nm for embedding the particle. We show first the computational result for water, a medium that has been most commonly used.

Figure 5a and b compare the 2-D temperature distributions calculated in water/glass and water/sapphire. Here, the calculation was made under the condition that Au NP is illuminated with a laser intensity of $I = 3.1$ mW μm^{-2} in water/glass and $I = 21.6$ mW μm^{-2} in water/sapphire. We used the following parameters: thermal conductivities of medium/substrate pairs, input amount of heat: Q[W] = I [W m^2] × C_{abs} [m^2] for a particle−substrate surface separation of +0.3 nm (Scheme 2c). Inspection of Figure 5a reveals that an axisymmetric temperature distribution with a distant-dependent decrease from the particle surface was obtained in water/glass. This axisymmetric temperature distribution should be achieved by modest

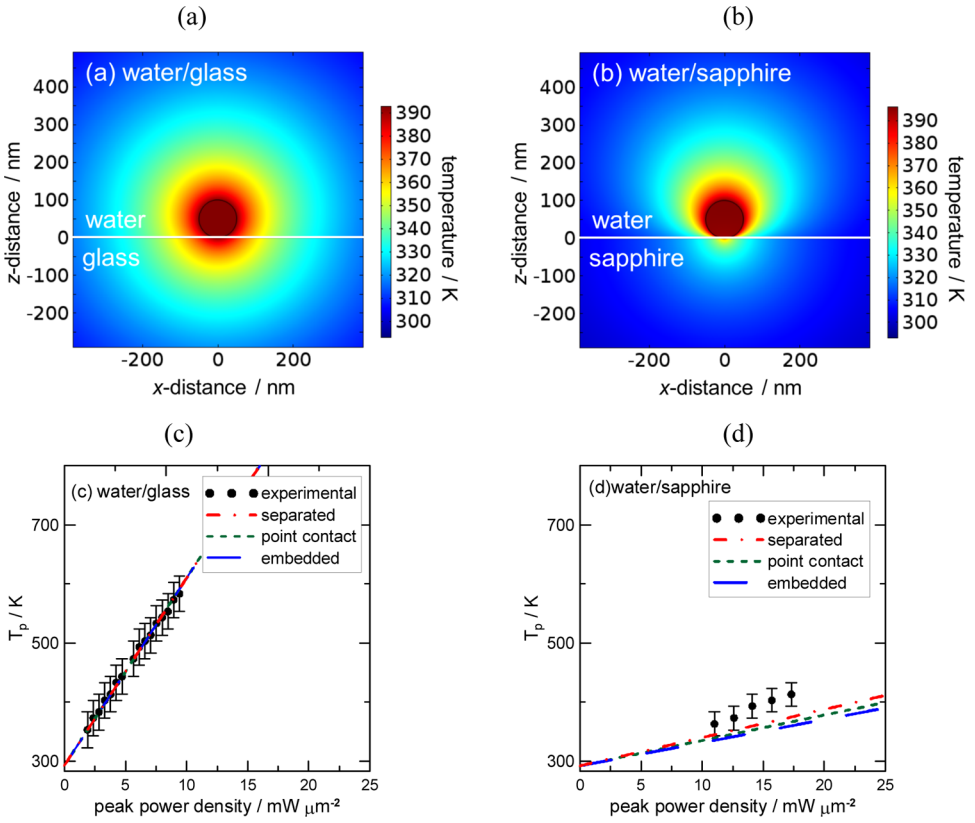

Figure 5. Computational 2-D temperature distributions for water/glass (a) and water/sapphire (b) and the calculated T_p as a function of laser intensity, *I*, for water/glass (c) and water/sapphire (d). In (a) and (b), a Au NP of 100 nm diameter was assumed to be separated from the substrate surface (the separation based on AFM measurement of the substrate surface and a monolayer thickness of the medium). The temperature distribution was obtained for a particle illuminated by the laser intensity $I = 3.1$ mW μm^{-2} for water/glass and $I = 21.6$ mW μm^{-2} for water/sapphire. The particle temperatures obtained are $T_p = 395$ K (a) and $T_p = 395$ K (b). In (c) and (d), three separation models given in Scheme 2 were applied (0.3 nm for all substrates). Experimental T_p is given in (c) and (d) for comparison.

disparity in the thermal conductivities of water and glass substrate. In marked contrast, in water/sapphire, the medium temperature exhibits a strong dependence on the direction from the particle center, as shown in Figure 5b. The medium at the lower side of a NP has appreciably lower temperatures than other areas presumably because of a considerable cooling exerted by the sapphire substrate with an appreciably higher thermal conductivity than water.

The particle temperatures calculated as a function of laser peak power densities were plotted for water/glass (Figure 5c) and water/sapphire (Figure 5d) systems. In both media, a good linear relationship was obtained for the calculated laser intensity *vs* particle temperature. However, a remarkable difference in the slope between water/glass and water/sapphire suggests that sapphire exhibits a great capability to cool the particle. The agreement of experimental and computational slopes is quite satisfactory, especially in water/glass; even for water/sapphire, the deviation in the slope is small. The three separation modes between the particle−substrate surfaces, *viz.*, point contact, embedded, and separated, were examined, and practically no differences were obtained by the calculation in water medium including the water/CaF_2 system (for water/CaF_2, Supporting Information S10). This can be explained by deducing that the thermal conductivity of water is high enough to compete with the substrate in cooling the particle, so that the medium exhibits a capability to transport heat to the substrate regardless of separation (this situation changes when air was used as a medium as discussed in the following). The good agreement of the experimental and computational particle temperature *vs* laser intensity relationships in water suggests the reliability of our temperature estimation method for substrates with various thermal conductivities. This is also the case in glycerol. As for water, the temperature *vs* laser intensity curves calculated were linear for glycerol, exhibiting a cooling effect slightly less than that for water. Note that also for glycerol no differences were obtained for the variation in the particle−substrate separation on the particle cooling effect (Supporting Information, S11).

As shown in Table 1, the most striking difference between k_{eff} and $\bar{k}$ (averaged values) was observed when we used sapphire substrate exposed in air. To figure out this discrepancy, we carried out the 2-D heat

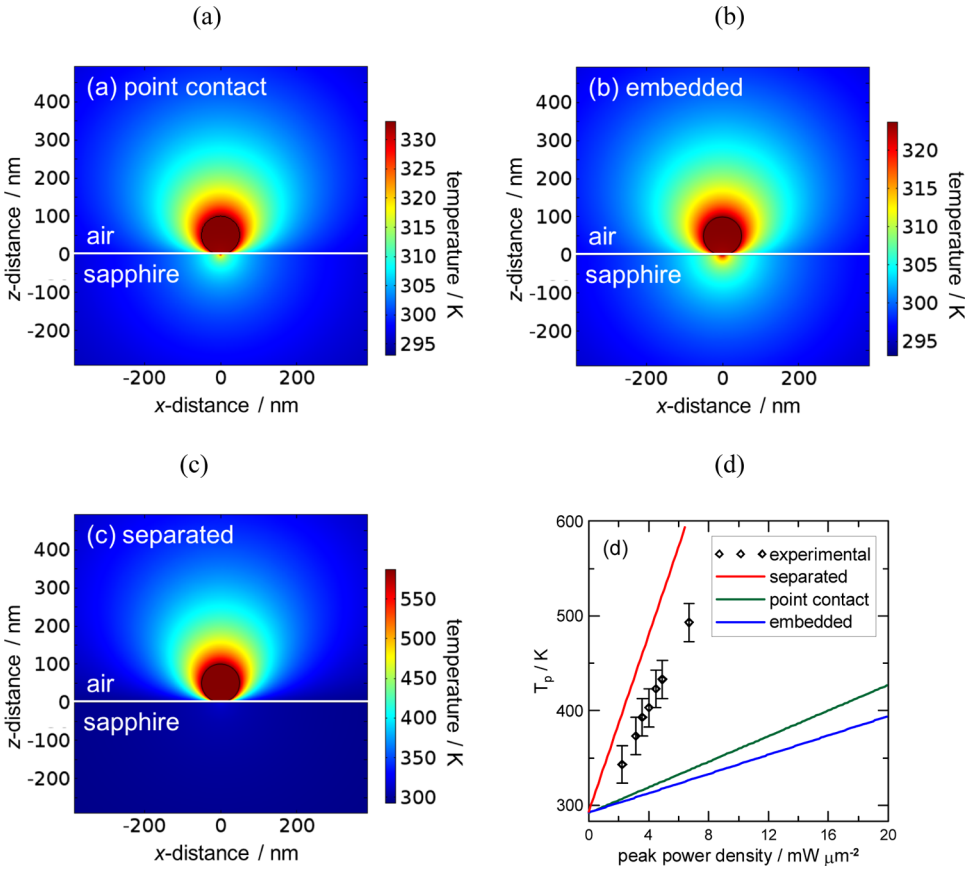

Figure 6. Computational 2-D temperature distributions for 100-nm-diameter Au NP in air/sapphire for three particle/substrate separations: point contact (a), 0.3 nm embedded (b), and 0.3 nm separated (c). The peak power density of 6.3 mW μm^{-2} was applied for the calculation of T_p in (a)−(c). The particle temperatures reached are 333 K (a), 324 K (b), and 587 K (c). Laser peak power density *vs* T_p relationship that shows the effect of particle−substrate separation on the temperature increase is given in (d).

conduction analysis and the calculation of the laser power density *vs* T_p relation, which leads to estimates of k_{eff} values. Figure 6 shows the 2-D temperature distributions in air/sapphire at three particle−substrate separations: point contact (0 nm separation), embedded (−0.3 nm embedded), and separated (+0.3 nm separated). For comparison purposes, experimental laser power density *vs* T_p data points is also shown. Inspection of Figure 6a−c reveals that the 2-D temperature distributions exhibit a remarkable anisotropy; the medium sides are well-heated, whereas the substrate sides are less heated because of the high thermal conductivity of sapphire, which acts as a particle coolant. Such a nonuniform 2-D temperature distribution from the disparity in the thermal conductivities of medium/substrate systems has been pointed out previously.[33] Notably, the particle−substrate separation gives a large difference in the temperatures at the interface between the particle and the substrate, on the substrate side. For instance, if they are in contact (a, b), a small hot spot is formed; in contrast, if separated (c), the substrate temperature remains cool. Furthermore, the temperature increase in air is greater when separated. Thus a big difference was obtained depending on the particle−substrate separation, which was not the case for other media: water and glycerol. To show more clearly the effect of particle−substrate separation, Figure 6d shows the computational particle temperature as a function of laser intensity. Whereas a temperature increase takes place with smaller gradients for systems where particle and substrate are in contact, a remarkably greater gradient was realized by separating the particle from the substrate. This difference arises from air's low thermal conductivity, which makes it act as a thermal insulator, preventing heat conduction to the substrate. The separated model gave a better agreement with the experimental laser intensity−particle temperature relationship.

We also carried out the temperature calculations in air/glass and air/CaF_2 systems. Figure 7a and b show the laser intensity *vs* T_p relationships in both systems (for typical 2-D temperature distributions for the three particle−substrate separation models in air/glass and air/CaF_2, see Supporting Information, S12). As air is being used as a surrounding medium, the particle temperatures are affected notably by particle−substrate separation as for sapphire. Most importantly,

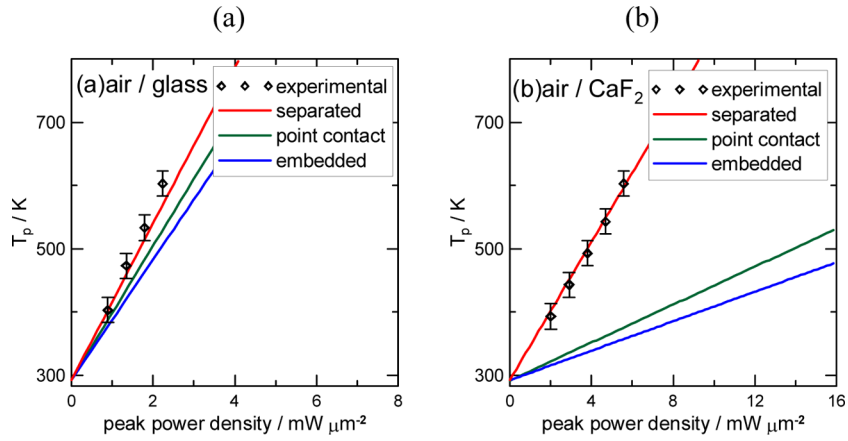

Figure 7. Computational particle temperature as a function of laser peak power density for a 100 nm diameter Au NP in air/glass and at different particle−substrate separations: point contact, 0.3 nm embedded, and 0.3 nm separated (a), and air/CaF_2 at different particle−substrate separations: point contact, 0.3 nm embedded, and 0.3 nm separated (b). For comparison, experimental laser intensity *vs* T_p relationships are given.

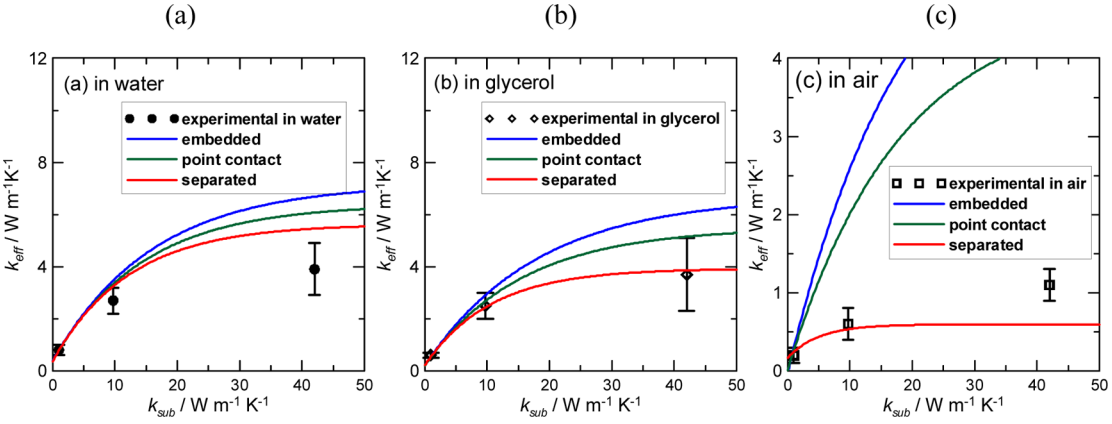

Figure 8. Experimental and computational k_{eff} *vs* k_{sub} curves for various substrates in three media: water (a), glycerol (b), and air (c).

the separated model gave a better agreement with the experiment, although not exactly the same. All the computational results presented above suggest that the Au NPs are sitting on the subnanometer-scale indented surface, and this serves to separate Au NPs from the substrate surface, interfering with the heat conduction through the substrate in the air environment. However, when we use water and glycerol as medium, this interface effect is minimal.

Experimental and Computational k_{eff} Values. We finally obtained a computation of k_{eff} from the gradients of the computed laser intensity *vs* T_p relationships. The results are listed in Table 1 and also plotted graphically in Figure 8 as a function of the thermal conductivity of the substrate, k_{sub}. Note that the k_{eff} values are obtained for the model in which Au NPs are supported on rough surfaces, and thus they are separated from the surface by 0.3 nm.

To date, a proper treatment of the effective thermal conductivity has been lacking for the supported systems.[9,13,34] The averaged thermal conductivity, $\bar{k}$, for the two-component system can be a good approximation when the thermal conductivity disparity between medium and substrate is minimal, such as for water and glass.[9,13] Yet, eq 2 is inadequate for a medium/substrate system in which a large disparity exists. To find a system that is properly treated by $\bar{k}$, we calculated the 2-D temperature distributions and laser peak power density *vs* T_p relationships for a 100 nm Au NP half-embedded in a substrate for glass, CaF_2, and sapphire in the three surrounding media (Supporting Information, S13). Despite the big disparity between k_{sub} and k_{med} in air/sapphire systems, we obtained axisymmetric temperature distributions that are similar to a homogeneous medium. More importantly, the calculated k_{eff} *vs* k_{sub} curves are linear and the slope is more or less similar to that of $\bar{k}$ *vs* k_{sub} curves regardless of k_{med} (Supporting Information, Fig S13-2). The result suggests that $\bar{k}$ should be used for the system in which a particle is half-embedded, not for a particle that is supported on a substrate.

The concept of k_{eff} obtained in the present study is best represented as a thermal conductivity "felt" or "sensed" by the Au NP itself, even though it is supported on a substrate in a medium, thus constituting a

complex environment. We emphasize that this is because the particle temperature is always uniform throughout the entire particle. Thus, the experimentally determined k_{eff} is meaningful for the particle, although this does not represent the actual inhomogeneous temperature distributions of the substrate/medium system outside the particle. Using this k_{eff} for a given laser intensity, we can determine the steady-state particle temperature that is useful in various experiments including surface-enhanced Raman spectroscopy and photothermal therapy.

CONCLUSION

We measured, as a function of laser intensity, the temperature of single 100-nm-diameter gold NPs, subjected to CW-laser illumination, supported on three differing substrates in three different media. We found that particle temperatures increase linearly with increasing laser intensity with strong dependence on both medium and substrate; the result points to various cooling effects occurring within the complex environment. The 1-D heat transfer model analysis of the experimental temperature−laser intensity relationship enabled the estimation of effective thermal conductivities (k_{eff}) for the nine substrate−medium pairs. The experimental k_{eff} values were in good agreement with those obtained by the numerical calculations solving the 2-D heat conduction equations. The computational study also revealed that a conventional $\bar{k}$ that was obtained by averaging the reported thermal conductivities of the two component values is a good approximation for a particle that is half-embedded in the substrate and half-exposed to the medium. Thus $\bar{k}$ is not appropriate for a particle supported on a substrate. For a precise representation of nanoscale heat transfer, we applied a 2-D heat transfer analysis, which revealed anisotropic temperature distributions. Nevertheless, the usefulness of the experimentally obtained k_{eff} values should not be underestimated, as k_{eff} can provide particle temperatures for a given excitation laser power regardless of the complexity of the system. In this report, we have shed light on the crucial role played by the substrate as well as the medium on nanoscale steady-state heating involving heat dissipation. A substrate in conjunction with the surrounding media can control particle temperature. This might find photothermal applications involving gold NPs in precision control of particle temperature under remote laser heating.

METHODS

Sample Preparation. Aqueous solutions of Au NPs with nominal diameters of 100 nm (cat. no. EMGC100, 100 ± 8 nm) were purchased from British Biocell International. Initially faceted, the particles were smoothed into spheres by irradiating with weak-intensity nanosecond laser pulses with a wavelength of 532 nm (~10 mJ cm^{-2}). The particle images acquired by a transmission electron microscope and the corresponding size distributions are given in the Supporting Information, Figure S1. The Au NPs were spin-coated onto a substrate that had been cleaned for 30 s on each side in a plasma reactor (Sakigake, YHS-R (70 W, 20 kHz)). The Au NPs were washed three times with doubly distilled water by placing in 0.5 mL of water and spun on a spin coater. Three types of substrate were employed: borosilicate glass (Schott D263T, 24 mm × 32 mm × 0.17 mm coverslip), sapphire (Furuuchi Chemical, 10 mm × 10 mm × 0.5 mm, optically polished on both sides), and CaF_2 (OKEN, 10 mm × 10 mm × 0.5 mm, optically polished on both sides). The Au NP-coated substrate was mounted on the scanning stage (Sigma, BIOS-105T, 100-nm resolution) of an optical microscope. In addition to this sample preparation, the Au NPs on a substrate were immersed in either water (doubly distilled) or glycerol (Merck, microscopy grade) in a 90 μL chamber consisting of two substrates separated by a 0.3-mm-thick silicone rubber spacer.

Optical Measurements. The forward light scattering spectra of single Au NPs were measured using a dark-field light microscopy−spectroscopy setup (Supporting Information, S14).[35−37] The spectra were obtained by subtracting the background signals including Raman scattering of the surrounding media and photoluminescence of the NP, then dividing it by the spectral profile of the white-light excitation source. Laser illumination was carried out through a microscope objective (60×, NA = 0.70) on an inverted microscope (Olympus IX 71 with a U-DCD dark-field condenser (NA = 0.8−0.92)) equipped with two output ports. The output from one port was relayed to a spectrograph consisting of an Acton SP300i polychromator (grating: 150 grooves/mm, blazed at 500 nm) and an Andor CCD camera (type: DU401-BR-DD operated at −60 °C) through a 300-μm-diameter pinhole, whereas the output from the other port was used for imaging with a digital camera (Nikon, DS-5M). The dark-field microscopy−spectroscopy was used to select a single particle that was subjected to laser illumination (typical particle images, Supporting Information, S14). Particles were brought to the laser spot by scanning a sample in the chamber on the motorized stage. The excitation of a single Au NP was performed using a focused 488 nm CW laser (NEOARK, TC20-4860-4.5) beam. The laser power was measured using a photodiode power meter (OPHIR, Orion). The spatial laser profile was determined by measuring scattering signal intensity of the 100-nm-diameter Au NP while scanning the stage at 100 nm intervals. The laser beam diameter thus determined was 1.2 μm, although a calculated $1/e^2$ diameter was 0.5 μm assuming a Gaussian beam profile and using experimental optical parameters (NA = 0.70, λ = 488 nm, n = 1.33). The laser peak power density I_p (mW μm^{-2}) was represent by[13]

$$I_p = \frac{P(2.3546)^2}{2\pi(\mathrm{FWHM})^2}$$

where P is the laser power density (measured laser power divided by beam area).

Numerical Calculations. A commercial finite-element mode solver, COMSOL Multiphysics v.4.3a (http://www.comsol.com), was employed for the calculations of 2-D temperature distributions in the medium and substrate and the evaluation of particle temperatures under the illumination of lasers with various intensities.

Conflict of Interest: The authors declare no competing financial interest.

Acknowledgment. Financial support from KAKENHI (No. 23310065, No. 25600026) is gratefully acknowledged. Dr. Takayuki Uwada of Josai University is acknowledged for his help with carrying out the numerical calculation of absorption cross sections.

Supporting Information Available: TEM micrographs of reshaped Au NPs, thermophysical and optical properties of media and substrates, fitting functions for the temperature-dependent

refractive indices of water and experimental $\Delta\lambda$ *vs* laser peak power density curves in water/glass, water/CaF_2, and water/sapphire, calculated spectral peak shift as a function of particle temperature of a 100-nm-diameter Au NP in various media, temperature profile, $T(r)$, when the finite interface resistivity was included or excluded from the CW-laser heating of a Au NP in a homogeneous medium, experimental and computational laser peak power density dependent T_p on three substrates in glycerol and air, absorption cross section obtained by Mie theory and numerical simulation, experimental and calculated scattering spectra of a d = 100 nm Au NP, computational procedure using COMSOL Multiphysics, surface roughness of glass, CaF_2, and sapphire substrates, 2-D temperature distribution and peak power density dependent T_p for a d = 100 nm Au NP immersed in water on a CaF_2 substrate, 2-D temperature distribution and peak power density dependent T_p for a d = 100 nm Au NP immersed in glycerol on glass, CaF_2, and sapphire substrates, 2-D temperature distributions dependent on the particle−substrate separation in air on glass and CaF_2 substrates, 2-D temperature distribution and k_{eff} as a function of k_{sub} for a d = 100 nm Au NP half-embedded in sapphire substrate exposed to air, glycerol, and water, and experimental setup and dark-field images of d = 100 nm Au NPs. This material is available free of charge *via* the Internet at http://pubs.acs.org.

REFERENCES AND NOTES

1. Qin, Z.; Bischof, J. C. Thermophysical and Biological Responses of Gold Nanoparticle Laser Heating. *Chem. Soc. Rev.* **2012**, *41*, 1191–1217.
2. Govorov, A. O.; Richardson, H. H. Generating Heat with Metal Nanoparticles. *Nano Today* **2007**, *2*, 30–38.
3. Baffou, G.; Quidant, R. Thermo-Plasmonics: Using Metallic Nanostructures as Nano-Sources of Heat. *Laser Photonics Rev.* **2013**, *7*, 171–187.
4. Dreaden, E. C.; Mackey, M. A.; Huang, X.; Kang, B.; El-Sayed, M. A. Beating Cancer in Multiple Ways Using Nanogold. *Chem. Soc. Rev.* **2011**, *40*, 3391–3404.
5. Dreaden, E. C.; Alkilany, A. M.; Huang, X.; Murphy, C. J.; El-Sayed, M. A. The Golden Age: Gold Nanoparticles for Biomedicine. *Chem. Soc. Rev.* **2012**, *41*, 2740–2779.
6. Plech, A.; Leiderer, P.; Boneberg, J. Femtosecond Laser Near Field Ablation. *Laser Photonics Rev.* **2009**, *3*, 435–451.
7. Hashimoto, S.; Werner, D.; Uwada, T. Studies on the Interaction of Pulsed Lasers with Plasmonic Gold Nanoparticles toward Light Manipulation, Heat Management, and Nanofabrication. *J. Photochem. Photobiol. C: Rev.* **2012**, *13*, 28–54.
8. Zijlstra, P.; Orrit, M. Single Metal Nanoparticles: Optical Detection, Spectroscopy and Applications. *Rep. Prog. Phys.* **2011**, *74*, 106401.
9. Hühn, D.; Govorov, A.; Gil, P. R.; Parak, W. J. Photostimulated Au Nanoheaters in Polymer and Biological Media: Characterization of Mechanical Destruction and Boiling. *Adv. Funct. Mater.* **2012**, *22*, 294–303.
10. Baffou, G.; Savatier, J.; Polleux, J.; Zhu, M.; Merlin, M.; Ringneault, H.; Monneret, S. Thermal Imaging of Nanostructures by Quantitative Optical Phase Analysis. *ACS Nano* **2012**, *6*, 2452–2458.
11. Fedoruk, M.; Lutich, A. A.; Feldmann, J. Subdiffraction-Limited Milling by an Optically Driven Single Gold Nanoparticle. *ACS Nano* **2011**, *5*, 7377–7382.
12. Skirtach, A. G.; Kurth, D. G.; Mohwald, H. Laser-Embossing Nanoparticles into a Polymeric Film. *Appl. Phys. Lett.* **2009**, *94*, 093106.
13. Carlson, M. T.; Khan, A.; Richardson, H. H. Local Temperature Determination of Optically Excited Nanoparticles and Nanodots. *Nano Lett.* **2011**, *11*, 1061–1069.
14. Honda, M.; Saito, Y.; Smith, N. I.; Fujita, K.; Kawata, S. Nanoscale Heating of Laser Irradiated Single Gold Nanoparticles in Liquid. *Opt. Express* **2011**, *19*, 12375–12383.
15. Bendix, P. M.; Reihani, S. N. S.; Oddershede, L. B. Direct Measurements of Heating by Electromagnetically Trapped Gold Nanoparticles on Supported Lipid Bilayers. *ACS Nano* **2010**, *4*, 2256–2262.
16. Setoura, K.; Werner, D.; Hashimoto, S. Optical Scattering Spectral Thermometry and Refractometry of a Single Gold Nanoparticle under CW Laser Excitation. *J. Phys. Chem. C* **2012**, *116*, 15458–15466.
17. Keblinski, P.; Cahill, D. G.; Bodapati, A.; Sullivan, C. R.; Taton, T. A. Limits of Localized Heating by Electromagnetically Excited Nanoparticles. *J. Appl. Phys.* **2006**, *100*, 054305.
18. Link, S.; El-Sayed, M. A. Size and Temperature Dependence of the Plasmon Absorption of Colloidal Gold Nanoparticles. *J. Phys. Chem. B* **1999**, *103*, 4212–4217.
19. Liz-Marzan, L. M.; Mulvaney, P. Au@SiO_2 Colloids: Effect of Temperature on the Surface Plasmon Absorption. *New J. Chem.* **1998**, *22*, 1285–1288.
20. Sumner, A. L.; Menke, E. J.; Dubowski, Y.; Newberg, J. T.; Penner, R. M.; Hemminger, J. C.; Wiegen, L. M.; Brauers, T.; Finlayson-Pitts, B. J. The Nature of Water on Surfaces of Laboratory Systems and Implications for Heterogeneous Chemistry in the Troposphere. *Phys. Chem. Chem. Phys.* **2004**, *6*, 604–613.
21. Tanabe, T.; Tatsuma, T. Plasmonic Manipulation of Color and Morphology of Single Silver Nanospheres. *Nano Lett.* **2012**, *12*, 5418–5421.
22. Mie, G. Beiträge zur Optik trüber Medien, Speziell Kolloidaler Metallösungen. *Ann. Phys.* **1908**, *25*, 377–445.
23. Bohren, C. F.; Huffman, D. R. *Absorption and Scattering of Light by Small Particles*; Wiley: New York, 1983.
24. Otter, M. Temperaturabhängigkeit der Optischen Konstanten Massiver Metalle. *Z. Phys.* **1961**, *161*, 539–549.
25. Baffou, G.; Quidant, R.; Javier, F.; Garcia de Abajo, F. J. Nanoscale Control of Optical Heating in Complex Plasmonic Systems. *ACS Nano* **2010**, *4*, 709–716.
26. Wilson, O. M.; Hu, X.; Cahill, D. G.; Braun, P. V. Colloidal Metal Particles as Probes of Nanoscale Thermal Transport in Fluids. *Phys. Rev. B* **2002**, *66*, 224301.
27. Juvé, V.; Scardamaglia, M.; Maioli, P.; Crut, A.; Merabia, S.; Joly, L.; Fatti, N. D.; Vallée, F. Cooling Dynamics and Thermal Interface Resistance of Glass-Embedded Metal Nanoparticles. *Phys. Rev. B* **2009**, *80*, 195406.
28. Merabia, S.; Shenogin, S.; Joly, L.; Keblinski, P.; Barrat, J.-L. Heat Transfer from Nanoparticles: A Corresponding State Analysis. *Proc. Natl. Acad. Sci. U.S.A.* **2009**, *106*, 15113–15118.
29. Baffou, G.; Rigneault, H. Femtosecond-Pulsed Optical Heating of Gold Nanoparticles. *Phys. Rev. B* **2011**, *84*, 035415.
30. Siems, A.; Weber, S. A .L.; Boneburg, J.; Plech, A. Thermodynamics of Nanosecond Nanobubble Formation at Laser-Induced Metal Nanoparticles. *New J. Phys.* **2011**, *13*, 043018.
31. Donner, J. S.; Baffou, G.; McCloskey, D.; Quidant, R. Plasmon-Assisted Optofluidics. *ACS Nano* **2011**, *5*, 5457–5462.
32. Opitz, A.; Scherge, M.; Ahmed, S. I.-U.; Schaefer, J. A. A Comparative Investigation of Thickness Measurements of Ultra-Thin Water Films by Scanning Probe Techniques. *J. Appl. Phys.* **2007**, *101*, 064310.
33. Baffou, G.; Quidant, R.; Girard, C. Thermoplasmonics Modeling: A Green's Function Approach. *Phys. Rev. B* **2010**, *82*, 165424.
34. Yamauchi, H.; Ito, S.; Yoshida, K.; Itoh, T.; Tsuboi, Y.; Kitamura, N.; Miyasaka, H. Temperature near Gold Nanoparticles under Photoexcitation: Evaluation Using a Fluorescence Correlation Technique. *J. Phys. Chem. C* **2013**, *117*, 8388–8396.
35. Mock, J. J.; Barbic, M.; Smith, D. R.; Schultz, D. A.; Schultz, S. Shape Effects in Plasmon Resonance of Individual Colloidal Silver Nanoparticles. *J. Chem. Phys.* **2002**, *116*, 6755–6759.
36. Sonnichsen, C.; Franzl, T.; Wilk, T.; von Plessen, G.; Feldmann, J.; Wilson, O.; Mulvaney, P. Drastic Reduction of Plasmon Damping in Gold Nanorods. *Phys. Rev. Lett.* **2002**, *88*, 077402.
37. Itoh, T.; Uwada, T.; Asahi, T.; Ozaki, Y.; Masuhara, H. Analysis of Localized Surface Plasmon Resonance by Elastic Light Scattering Spectroscopy of Individual Au Nanoparticles for Surface Enhanced Raman Scattering. *Can. J. Anal. Sci. Spectrosc.* **2007**, *52*, 130–141.